Geosci. Model Dev. Discuss., 8, 209–262, 2015
www.geosci-model-dev-discuss.net/8/209/2015/
doi:10.5194/gmdd-8-209-2015

Geoscientific Model Development Discussions
Open Access

A two-layer canopy with thermal inertia for an improved modelling of the sub-canopy snowpack energy-balance

I. Gouttevin[1,2], M. Lehning[2,3], T. Jonas[3], D. Gustafsson[4], and M. Mölder[5]

[1]IRSTEA, Unité de Recherche Hydrologie-Hydraulique, 5 rue de la Doua, CS 70077, 69626 Villeurbanne CEDEX, France
[2]CRYOS, School of Architecture, Civil and Environmental Engineering, EPFL, Lausanne, Switzerland
[3]WSL Institute for Snow and Avalanche Research SLF, Flüelastrasse 11, 7260 Davos Dorf, Switzerland
[4]KTH, Department of Land and Water Resources engineering, Stockholm, Sweden
[5]Lund University, Department of Physical geography and Ecosystem science, Sölvegatan 12, 223 62 Lund, Sweden

Received: 16 October 2014 – Accepted: 25 November 2014 – Published: 13 January 2015

Correspondence to: I. Gouttevin (isabelle.gouttevin@irstea.fr)

Published by Copernicus Publications on behalf of the European Geosciences Union.

Abstract

A new, two-layer canopy module with thermal inertia as part of the detailed snow model SNOWPACK (version 3.2.1) is presented and evaluated. This module is designed to reproduce the difference in thermal response between leafy and woody canopy elements, and their impact on the underlying snowpack energy balance. Given the number of processes resolved, the SNOWPACK model with its enhanced canopy module constitutes a very advanced, physics-based atmosphere-to-soil-through-canopy-and-snow modelling chain.

Comparisons of modelled sub-canopy thermal radiation to stand-scale observations at an Alpine site (Alptal, Switzerland) demonstrate the improvements of the new canopy module. Both thermal heat mass and the two-layer canopy formulation contribute to reduce the daily amplitude of the modelled canopy temperature signal, in agreement with observations. Particularly striking is the attenuation of the night-time drop in canopy temperature, which was a key model bias. We specifically show that a single-layered canopy model is unable to produce this limited temperature drop correctly.

The impact of the new parameterizations on the modelled dynamics of the sub-canopy snowpack is analysed and yields consistent results but the frequent occurrence of mixed-precipitation events at Alptal prevents a conclusive assessment of model performance against snow data.

The new model is also successfully tested without specific tuning against measured tree temperatures and biomass heat storage fluxes at the boreal site of Norunda (Sweden). This provides an independent assessment of its physical consistency and stresses the robustness and transferability of the parameterizations used.

1 Introduction

In the Northern Hemisphere, around 19 % of the annually snow-covered areas are forested (Rutter et al., 2009). As this type of ecosystem has considerable implications for the mass and energy balance of the surface snowpack (e.g. Harding and Pomeroy, 1996; Otterman et al., 1988), the proper understanding and representation of the snow-canopy interactions is crucial whenever realistic estimates of snow cover and melt dynamics in forested environments are needed. This is specifically of concern for hydrological modelling at all scales, runoff estimates from poorly gauged catchments, flood and drought forecasting, global water budget assessment, and in support of local water resources management including irrigation, provision of drinking water, industrial, touristic or hydropower applications.

Also, the snowpack insulates the underlying soil from winter cold air temperatures, with implications for the ecosystem in terms of vegetation cover and dynamics (Rasmus et al., 2011; Grippa et al., 2005), litter decomposition (e.g. Saccone et al., 2013) or carbon cycling (e.g. Kelley et al., 1968). The representation of this insulation is one of the critical uncertainties of the modelling of the global soil carbon cycle and its evolution in permafrost environments (Lawrence and Slater, 2010; Gouttevin et al., 2012). The northwards migration of shrubs observed in the last decades at high latitudes (e.g. ACIA, 2005) also indicates that snow-forest interactions are to become more and more a concern for climate modelling in the context of global warming.

The insulation properties of snow depend on snow depth and snow thermal conductivity, which in the end relates to the type, characteristics and spatial arrangement of snow crystals within the snowpack. The realistic description of these parameters can hence be a prerequisite for a reliable representation of soil thermal regime and microbiological processes. Snow stratigraphy is also of concern for specific local activities like reindeer grazing in northern countries (Tyler et al., 2010; Vikhamar-Schuler et al., 2013). At present, to the author's knowledge, such a description is rarely provided by modelling tools for sub-canopy snowpacks (Rasmus et al., 2007; Tribbeck et al., 2006).

Several processes affect the snow cover in sub-canopy environments when compared to open sites. Snow interception by dense canopies and subsequent sublimation or melt of intercepted snow, can reduce sub-canopy snow accumulation by up to 60 % (Hardy et al., 1997). Conversely, canopy shading from solar shortwave radiations (SW)

GMDD
8, 209–262, 2015

can lead to longer-lasting snow cover in forested environments, while enhanced longwave emissions (LW) from sunlit trees with low albedo can have the reverse effect (Sicart et al., 2004; Strasser et al., 2011; Lundquist et al., 2013). In such an environment, effects by topographical shading, solar angle, canopy structure, and understory further complicate matters. Sub-canopy snow is additionally sheltered from wind, thereby experiencing reduced turbulent fluxes. This complexity makes the understanding and prediction of the sub-canopy snow cover evolution a challenging task.

In line with recent thinking in hydrological modelling (Sivapalan et al., 2003), Rutter et al. (2009) hinted that the consideration of canopy processes in snow models (rather than calibration of parametric models) offers the best possibility to address the above-mentioned hydrological and ecosystemic challenges in a manner that ensures site-transferability and robustness with respect to changing climate. Existing models linking a comprehensive, physics-based representation of the canopy to the evolution and properties of the underlying snowpack, are rare: the SNOWCAN model (Tribbeck et al., 2004, 2006) couples a robust radiative transfer model for canopies to the detailed snowpack model SNTHERM. However, this modelling chain is not fully comprehensive as it relies on canopy temperature provided as input to represent the canopy thermal emissions, which can substantially contribute to sub-canopy snowmelt (Adams et al., 1996). Furthermore, SNOWCAN proposes coarse parameterizations for interception and turbulent processes, which are not critical for snowmelt but can be determinant in the accumulation phase. The COUP model (Jansson and Karlberg, 2001) features an advanced representation of snow-canopy processes but lacks a detailed, layered snowpack and the associated physical processes. In their design of a land surface model dedicated to intensively cold regions, Yamazaki et al. (1992); Yamazaki (2001) resolve the forest energy balance for two canopy layers (crown and trunks). However, they do not assess specifically the added value of this model design for the sub-canopy snow surface energy balance. Also, their snow model is of intermediate complexity.

We here further develop the SNOWPACK model (Bartelt and Lehning, 2002; Lehning et al., 2002, 2006), which proposes a very detailed, physical and microphysical representation of the snowpack, and also includes a simple canopy module where radiation and precipitation interception by forest elements are represented (e.g. Rutter et al., 2009; Musselmann et al., 2012). With the enhanced physical representation of canopy processes that we propose, it builds one of the few comprehensive and detailed physics-based formulations of the soil-snow-canopy-atmosphere continuum, of value for applications ranging from hydrology to ecosystem modelling and understanding.

In the SnowMIP2 study, Rutter et al. (2009) demonstrate the potential for improvement of snow-forest process-based models: they highlight among others the misrepresentation of ablation events driven by air temperature rising above 0 °C, when models diverge from observations due to their treatment of sub-canopy longwave radiations. This effect, and the importance of accounting for the thermal structure of different canopy elements, has been pinpointed before by other observation-based studies (Pomeroy et al., 2009; Sicart et al., 2004). A consistent modelling the sub-canopy thermal radiations and their impact on the underlying snowpack was lacking in SNOWPACK, and is therefore the focus of the present study.

The developments presented and documented in this contribution feature a two-layer formulation of the canopy accounting for the different temperatures of leafy and woody elements, and a representation of the canopy thermal inertia. The description of these developments is embedded in a full documentation of the SNOWPACK canopy module, earlier versions of which have been partially described in Stähli et al. (2006) and in appendix A of Musselmann et al. (2012). The added value of the new model features for the sub-canopy snowpack energy balance is demonstrated against two observational datasets from a temperate Alpine forest site (Alptal, Switzerland) and a boreal forest site (Norunda, Sweden).

2 Model description

2.1 The SNOWPACK/Alpine3D snow model

SNOWPACK is a one-dimensional, physics-based snow-cover model originally dedicated to avalanche risk assessment. Driven by standard meteorological observations, the model describes the stratigraphy, snow microstructure, snow metamorphism, temperature distribution, and settlement as well as surface energy exchange and mass balance of a seasonal snow cover. It has been extensively described in Bartelt and Lehning (2002) and Lehning et al. (2002a, b). Since 2005, it also includes the effect of vegetation above and within or below the snowpack.

Snowpack can be wrapped into an open-source, spatially distributed, 3-dimensional model for analyzing and predicting the dynamics of snow-dominated surface processes in complex alpine topographies: Alpine3D (Lehning et al., 2006). In addition to SNOWPACK, Alpine3D includes an interpolation module for meteorological fields (including radiations as affected by topography, Helbig et al., 2009), an optional snow transport model (Lehning et al., 2008) and an optional runoff model (Zappa et al., 2003). The interpolated or provided spatial meteorological fields drive the energy and mass balance of the surface snowpack, computed by SNOWPACK. The canopy module and its new features described hereafter can run within Alpine3D.

2.2 The canopy model structure

The canopy module of SNOWPACK calculates the upper boundary conditions for the snowpack or bare soil surface below the canopy. It is based on an energy balance approach in order to be consistent with the distributed radiation scheme used in Alpine3D. Interception and throughfall of precipitation, transpiration and evaporation of intercepted snow or rain, as well as the influence of the canopy on radiative and turbulent heat fluxes at the snow or soil surface, are included in the model.

GMDD
8, 209–262, 2015

In its 1-layer version, the model represents vegetation canopy as a single big-leaf with state variables (i) canopy temperature T_{can} (K) and (ii) storage of intercepted water or snow I (mm). All canopy processes are then computed based on three basic input parameters: canopy height z_{can} (m), leaf area index LAI or plant area index PAI ($m^2\,m^{-2}$), and direct throughfall fraction c_f (–). PAI has more of a physical sense as non-leafy canopy elements play a role in radiative extinction and turbulent fluxes, but PAI and LAI can usually be derived from each other via a factor depending on stand characteristics, thus the switch between both just affects parameter values in our formulations. The description here uses LAI; the direct throughfall fraction can be set to zero if LAI is provided as a stand-scale average including canopy gaps of moderate size (up to ~ 1 m). These 3 model parameters intend to describe differences between forest stands without further tuning.

The consideration of the thermal inertia of the forest stand in the 1-layer version with heat mass (1LHM) and the 2-layer version (2LHM) imposes the use of an additional input parameter, the mean stand basal area B ($m^2\,m^{-2}$). The different parameters used by the SNOWPACK canopy module are listed in Table 1, distinguishing between the ones to be provided by users according to forest-specificities, and the ones internal to the model.

The 2-layer version is meant reproduce the thermal contrast between the outermost canopy part (leaves or needles), which is most directly exposed to the atmosphere, and the inner part of the canopy (twigs, branches, trunks, some leaves), for which energy and mass fluxes have already been altered by the outermost canopy part. This modelling choice relies on observational data highlighting this contrast and its relevance for the sub-canopy energy balance (Pomeroy et al., 2009). With respect to the 1-layer version, one state variable is added, namely the temperature of the trunk or inner-canopy T_{trunk} (K). T_{can} is then replaced by T_{leaves}, the temperature of the outer canopy.

The coupled water and heat balances of the canopy layer are calculated in three steps:

GMDD
8, 209–262, 2015
A two-layer canopy with thermal inertia
I. Gouttevin et al.

1. First, a preliminary mass balance is calculated including interception and throughfall of precipitation.

2. Second, the canopy temperature T_{can} is calculated by solving the energy balance of the canopy. For this purpose, all the non-linear energy fluxes to the canopy have been linearized in terms of canopy temperature via Taylor series. The radiation transfer and turbulent exchange of sensible and latent heat are then deduced. For the 2-layer version, the energy balance of the outer canopy also includes thermal emissions from the inner canopy, which are similarly linearized in terms of T_{can} via the explicit formulation of an energy balance for the inner canopy.

3. Third, the mass balance of the canopy is updated by the evaporation (or condensation) calculated in step two.

The 2-layer version affects the canopy energy balance and computation of net radiation in each layer. For the sake of simplicity the 1-layer canopy module is first fully described. The specificities implied by the consideration of two layers are then dealt with in the last part of this section.

2.3 Interception parameterization

The mass balance of the canopy layer includes three fluxes of water: interception of precipitation ΔI (mm day^{-1}), interception evaporation E_{int} (mm day^{-1}) and water unloading from the canopy U (mm day^{-1}):

$$dI/dt = \Delta I - E_{int} - U. \quad (1)$$

where I (mm) is the interception storage.

A fraction $(1-c_f)$ of the precipitation P (mm day^{-1}) is available for interception at each time step. The interception rate is calculated as a function of canopy storage saturation with an equation originally proposed by Merriam (1960), in the form given by Pomeroy et al. (1998):

$$\Delta I = c(I_{\max} - I)\left(1 - \exp\left\{-\frac{(1-c_f)P}{I_{\max}}\right\}\right). \tag{2}$$

where the parameter c (–) is a model time-step dependent parameter known as the unloading coefficient. Pomeroy et al. (1998) suggested a value of $c = 0.7$ appropriate for hourly time-steps. Canopy interception capacity $I_{\max}$ (mm) is assumed to be proportional to leaf area index:

$$I_{\max} = i_{\mathrm{LAI}}\mathrm{LAI} \tag{3}$$

where the parameter i_{LAI} (mm) is either set to a constant corresponding to the interception capacity for liquid precipitation when these occur, or parameterized as a function of snow density during snowfall events, following Pomeroy et al. (1998):

$$i_{\mathrm{LAI}} = i_{\max}(0.27 + 46/\rho_{\mathrm{s,\,int}}). \tag{4}$$

Schmidt and Gluns (1991) reported estimates of the parameter $i_{\max}$ (mm) for spruce (5.9) and pine (6.6). The density of the intercepted snow $\rho_{\mathrm{s,\,int}}$ ($\mathrm{kg\,m^{-3}}$) is estimated as a function of air temperature (Lehning et al., 2002b). Different values have been reported for the interception capacity of snow, depending on forest type and climate (e.g. Koivusalo et al., 2002; Essery et al., 2003). Most important is to recognize the large difference between frozen and liquid precipitation. The quality of the intercepted water is assumed to be equal to the quality of precipitation at each timestep, i.e. no explicit simulation of snow melt or snow densification in the canopy is included in the model.

The partition of precipitation into snowfall and rainfall in SNOWPACK depends on available data. Usually precipitation with undistinguished phase is used, and a temperature threshold disentangles the phases, possibly with linear or logistic smoothing around the threshold (Kavetski and Kuczera, 2007). When phase information is

GMDD
8, 209–262, 2015

available and mixed events occur, the interception capacity is calculated according to Eq. (4), but using the weighed sum of liquid water and new snow density instead of the density of snow. For rain-only or snow-only events, Eqs. (3) and (4) are respectively used without change.

Different approaches have been proposed for calculations of snow unload from the canopy: Essery et al. (2003) set the unload rate equal to a fraction (40 %) of calculated melt of intercepted snow. Koivusalo and Kokkonen (2002) assumed that all intercepted snow unloads as soon as the air temperature rises above 0 °C. We have chosen to calculate snow unload U (mm day^{-1}) only when the interception storage exceeds the actual interception capacity:

$$U = \max[0, I - I_{\max}]/\Delta t, \tag{5}$$

which happens when the capacity is reduced due to an air temperature increase. Sudden release of large amount of snow is thus avoided since the intercepted snow density is increased gradually towards the threshold air temperature for snowfall, which is favorable for the numerical stability of the snowpack simulation. This simple parameterization also respects the fact that individual branches usually release snow at a time and total unloading of a whole tree is not very frequent.

Throughfall T (mm day^{-1}) to the forest floor is thus equal to:

$$T = P - \Delta I + U \tag{6}$$

Evaporation of intercepted water is calculated as part of the canopy energy balance (cf. below) and added to the water balance at the end of the model time step.

2.4 Canopy energy balance

The canopy temperature is directly derived from the canopy energy balance.

The 1-layer canopy module with no heat mass (1LnoHM, e.g. the version used in previous modelling studies: Rutter et al., 2009; Musselmann et al., 2012) relies on

GMDD
8, 209–262, 2015

an assumption of stationarity, whereby net radiation of the canopy $R_{\text{net, can}}$ (W m^{-2}) is assumed to equal the sum of sensible H_{can} (W m^{-2}) and latent LE_{can} (W m^{-2}) heat fluxes neglecting any storage or sources/sinks of heat within the canopy:

$$R_{\text{net, can}} = H_{\text{can}} + \text{LE}_{\text{can}} \tag{7}$$

In the new canopy module, 1 layer version with heat mass, (1LHM) the thermal inertia of trees is accounted for via a biomass storage flux BM_{can} (W m^{-1}), modifying the canopy energy balance:

$$R_{\text{net, can}} = H_{\text{can}} + \text{LE}_{\text{can}} + \text{BM}_{\text{can}} \tag{8}$$

2.4.1 Radiation transfer

A radiation transfer model for a single canopy layer above a snow or bare soil surface has been adopted from Taconet et al. (1986) by Stähli et al. (2009). The model assumes a fractional absorption of radiation in the canopy layer given by the absorption factor σ_{f} (–). A fraction of the absorbed radiation is reflected, as defined by the reflection factors for shortwave (albedo) and longwave radiation, respectively. Radiation transmitted to the surface below is absorbed and reflected according to the corresponding reflection factors for the surface.

Following these basic assumptions, and integrating n multiple reflections between the canopy layer and the underlying surface, the net shortwave radiation absorbed by the canopy layer $\text{SW}_{\text{net, can}}$ (W m^{-2}) is given by:

$$\begin{aligned}\text{SW}_{\text{net, can}} = {} & \text{SW}_{\downarrow} - \sigma_{\text{f}}\alpha_{\text{can}}\text{SW}_{\downarrow} - (1-\sigma_{\text{f}})\text{SW}_{\downarrow} \\ & + \sum_{n=1}^{\infty}(\alpha_{\text{surf}})^n(\sigma_{\text{f}}\alpha_{\text{can}})^{n-1}(1-\sigma_{\text{f}})\text{SW}_{\downarrow} \\ & - \sum_{n=1}^{\infty}(\alpha_{\text{surf}})^n(\sigma_{\text{f}}\alpha_{\text{can}})^{n}(1-\sigma_{\text{f}})\text{SW}_{\downarrow}\end{aligned}$$

GMDD
8, 209–262, 2015

A two-layer canopy with thermal inertia

I. Gouttevin et al.

$$
-\sum_{n=1}^{\infty}(\alpha_{\text{surf}})^{n}(\sigma_{\text{f}}\alpha_{\text{can}})^{n-1}(1-\sigma_{\text{f}})^{2}\text{SW}_{\downarrow} \tag{9}
$$

where $\text{SW}_{\downarrow}$ (W m^{-2}) is the incoming shortwave radiation above the canopy layer, and α_{can} (–) and α_{surf} (–) are the albedo of the canopy and the snow/soil surface below, respectively. The first three terms on the right hand side are the incident, reflected, and transmitted downward radiation with regard to the canopy layer. The remaining three terms are the sums of incident, reflected and transmitted upward radiation, as a result of multiple reflections between the canopy and the surface below. Equation (9) can be simplified to:

$$
\text{SW}_{\text{net, can}} = \text{SW}_{\downarrow}(1-\alpha_{\text{can}})\sigma_{\text{f}}\left(1+\frac{\alpha_{\text{surf}}(1-\sigma_{\text{f}})}{1-\sigma_{\text{f}}\alpha_{\text{surf}}\alpha_{\text{can}}}\right) \tag{10}
$$

by mathematical relationships for geometric series. The same procedure can be applied for net shortwave radiation absorbed by the ground surface $\text{SW}_{\text{net, surf}}$ (W m^{-2}), which thus can be written as:

$$
\text{SW}_{\text{net, surf}} = \frac{\text{SW}_{\downarrow}(1-\alpha_{\text{surf}})(1-\sigma_{\text{f}})}{1-\sigma_{\text{f}}\alpha_{\text{surf}}\alpha_{\text{can}}} \tag{11}
$$

The calculation of the longwave radiation is further simplified by assuming an emissivity equal to 1, giving the following equations for net longwave radiation absorbed by the canopy $\text{LW}_{\text{net, can}}$ (W m^{-2}), and the ground surface $\text{LW}_{\text{net, surf}}$ (W m^{-2}):

$$
\text{LW}_{\text{net, can}} = \sigma_{\text{f}}(\text{LW}_{\downarrow}+\sigma T_{\text{surf}}^{4}-2\sigma T_{\text{can}}^{4}) \tag{12}
$$

$$
\text{LW}_{\text{net, surf}} = (1-\sigma_{\text{f}})\text{LW}_{\downarrow}+\sigma_{\text{f}}\sigma T_{\text{can}}^{4}-\sigma T_{\text{surf}}^{4} \tag{13}
$$

where σ is the Stefan–Bolzman constant $5.67\times10^{-8}\,\text{W m}^{-2}\,\text{K}^{-4}$ and $\text{LW}_{\downarrow}$ is the thermal radiations from the sky. Neglecting the emissivity might overestimate the loss and gain

GMDD
8, 209–262, 2015
A two-layer canopy with thermal inertia
I. Gouttevin et al.

of thermal radiation from the canopy. On the other hand, the absorption factor σ_f (–) has a similar effect on the net adsorption/emittance, and it may be difficult to separate these two properties in the case of longwave radiation.

The net radiation to the canopy is then the sum of the LW and SW net contributions:

$$R_{\text{net, can}} = \text{SW}_{\text{net, can}} + \text{LW}_{\text{net, can}} \tag{14}$$

The albedo of the canopy α_{can} (–) is equal to:

$$\alpha_{\text{can}} = f_{\text{wet}}\alpha_{\text{wet}} + (1 - f_{\text{wet}})\alpha_{\text{dry}} \tag{15}$$

where f_{wet} (–) is the fraction of the canopy covered by intercepted water calculated as:

$$f_{\text{wet}} = (I/I_{\max})^{2/3}, \tag{16}$$

and α_{wet} (–) and α_{dry} (–) are the albedo of wet and dry canopy, respectively. The albedo for the wet part of the canopy can be set differently for liquid and frozen interception (Table 1).

The canopy absorption factor σ_f (–) is assumed to be equal for longwave and diffuse shortwave radiation, independent of interception storage and quality, and is calculated as a function of LAI:

$$\sigma_f = 1 - \exp\{-k_{\text{LAI}}\text{LAI}\} \tag{17}$$

where k_{LAI} (–) is an extinction parameter with values normally between 0.4–0.8.

For direct shortwave radiations, it can optionally be a function of solar elevation angle θ_{elev}, following Chen et al. (1997):

$$\sigma_{\text{f, dir}} = 1 - \exp\left\{-\frac{k_{\text{LAI}}\text{LAI}}{\sin(\theta_{\text{elev}})}\right\} \tag{18}$$

where θ_{elev} is limited to the range $[0.001 - \pi/2]$ to ensure a positive value of $\sigma_{\text{f, dir}}$.

GMDD
8, 209–262, 2015

A two-layer canopy with thermal inertia

I. Gouttevin et al.

Direct and diffuse SW radiations are in this case disentangled by the model after Erbs et al. (1982).

For the sake of completeness, the effective surface albedo, α_{total} (–), and radiative surface temperature, T_{eff} (K) above the canopy layer are given as:

$$\alpha_{\mathrm{total}} = \alpha_{\mathrm{can}}\sigma_{\mathrm{f}} + \alpha_{\mathrm{surf}}\frac{(1-\sigma_{\mathrm{f}})^2}{1-\alpha_{\mathrm{can}}\alpha_{\mathrm{surf}}\sigma_{\mathrm{f}}} \tag{19}$$

and

$$T_{\mathrm{eff}} = \left(\frac{\mathrm{LW}_{\downarrow} - \mathrm{LW}_{\text{net, can}} - \mathrm{LW}_{\text{net, surf}}}{\sigma}\right)^{0.25} \tag{20}$$

respectively. These variables have no influence on the 1-D-simulations presented here, but are used to estimate the contribution of longwave and shortwave radiation from surrounding terrain when the SNOWPACK model is used within the distributed Alpine3D model.

Finally, the radiation fluxes calculated by the canopy module are only applied to the fraction of the surface covered by the canopy, assumed to be the complement of the direct throughfall parameter: $(1-c_{\mathrm{f}})$. An exception to that occurs for direct shortwave which is collimated in the solar direction and can encounter a fraction of forest larger than $(1-c_{\mathrm{f}})$ at sub-zenithal solar angles. This higher fraction of canopy shading $(1-c_{\mathrm{f,dir}})$ is derived following Gryning et al. (2001) from the mean canopy height z_{can} (m) and an average canopy diameter D_{can} (1 m by default):

$$1-c_{\text{f, dir}} = \mathrm{Min}\left[1, (1-c_{\mathrm{f}})\cdot\left(1+\frac{4\times z_{\mathrm{can}}}{\pi\cdot D_{\mathrm{can}}\cdot\tan(\theta_{\mathrm{elev}})}\right)\right] \tag{21}$$

In the remaining fraction of the surface, the exchange of longwave and shortwave radiation between the atmosphere and the ground surface is calculated without influence of the canopy.

GMDD
8, 209–262, 2015

2.4.2 Turbulent fluxes

The turbulent fluxes of sensible and latent heat from the canopy to the reference level of the meteorological input above the canopy are calculated using the bulk formulation:

$$H_{\mathrm{can}} = \frac{\rho c_p}{r_{\mathrm{H}}}(T_{\mathrm{can}} - T_{\mathrm{air}}) \tag{22}$$

$$\mathrm{LE}_{\mathrm{can}} = \frac{0.622L}{R_{\mathrm{a}}T_{\mathrm{air}}}\frac{1}{r_{\mathrm{E}}}(e_{\mathrm{sat}}[T_{\mathrm{can}}] - e_{\mathrm{air}}) \tag{23}$$

where ρ (kg m^{-3}) and c_p (J kg^{-1} K^{-1}) are the density and heat capacity of air, T_{can} (K) is the canopy layer temperature, T_{air} (K) and e_{air} (Pa) are the air temperature and the actual vapour pressure in the air at a reference level z_{ref} (m) above the ground surface, L (J kg^{-1}) is the latent heat of vaporization of water (or sublimation when $T_{\mathrm{air}} < 273.15$ K), R_{a} is the specific gas constant for air (J kg^{-1} K^{-1}), and $e_{\mathrm{sat}}[T_{\mathrm{can}}]$ (P_{a}) is the saturated vapour pressure corresponding to the canopy temperature. Furthermore, the turbulent transfer coefficients for heat and vapour are expressed in terms of the aerodynamic resistances r_{H} (s m^{-1}) and r_{E} (s m^{-1}) (further described below). Latent heat flux is the sum of transpiration E_{tr} (mm s^{-1}) and evaporation of intercepted water E_{int} (mm s^{-1}). The partitioning of the components from partly wet canopies can be a delicate problem. To simplify the numerical solution of the energy balance, we have chosen to formulate an effective aerodynamic resistance for latent heat calculated as an average of the corresponding values for transpiration r_{Etr} and interception evaporation r_{Eint}, weighted by the fraction of wet canopy f_{wet}:

$$\frac{1}{r_{\mathrm{E}}} = \frac{1}{r_{\mathrm{Eint}}}f_{\mathrm{wet}} + \frac{1}{r_{\mathrm{Etr}}}(1 - f_{\mathrm{wet}}) \tag{24}$$

GMDD
8, 209–262, 2015

whereby the total evaporation E_{can} ($\mathrm{m\,day^{-1}}$) is calculated directly, and the components are derived as secondary results:

$$E_{\mathrm{int}} = E_{\mathrm{can}} \frac{r_{\mathrm{E}}}{r_{\mathrm{Eint}}} f_{\mathrm{wet}} \tag{25}$$

$$E_{\mathrm{tr}} = E_{\mathrm{can}} \frac{r_{\mathrm{E}}}{r_{\mathrm{Etr}}} (1 - f_{\mathrm{wet}}) \tag{26}$$

The derivation of the aerodynamic resistances for transpiration and interception evaporation is given in the next section. Transpiration is not allowed if the achieved $\mathrm{LE}_{\mathrm{can}}$ is negative (i.e. condensation), therefore in such cases, the solution of the energy balance has to be re-calculated using $f_{\mathrm{wet}} = 1$.

At temperatures below the freezing point the modelled canopies do not transpire anymore. If the canopy energy balance forces, through Eq. (24), an evaporation that cannot be sustained by the interception storage, the latter limits the possible evaporation and the canopy energy balance is recalculated accordingly.

2.4.3 Aerodynamic resistances

The aerodynamic resistances for sensible and latent heat fluxes are calculated using a two-layer model adapted from Blyth et al. (1999), which for simplicity assumes logarithmic or log-linear wind profiles both above, within, and below the canopy. More elaborate models have been suggested by for instance Shuttleworth and Wallace (1985), however, the remaining uncertainties in the representation of the within-canopy turbulent exchange calls for a simple approach. The aerodynamic resistance for scalars from the canopy level, defined by the displacement height d (m), to the reference level of the wind and temperature measurements z_{ref} above the canopy, is calculated as:

$$1/r_{\mathrm{air}} = u_{*}k / \left(\ln\left(\frac{z_{\mathrm{ref}} - d}{z_{0\mathrm{m}}}\right) + \psi_{\mathrm{h}} \right) + c_{\mathrm{h0}} / \left(\rho c_{p}\right) \tag{27}$$

where u_* ($\mathrm{m\,s^{-1}}$) is the friction velocity:

$$u_* = u_{\mathrm{ref}} k \Big/ \left(\ln\left(\frac{z_{\mathrm{ref}} - d}{z_{0\mathrm{m}}}\right) + \psi_\mathrm{m} \right) \tag{28}$$

k is the Karman constant (0.4), $z_{0\mathrm{h}}$ (m) and $z_{0\mathrm{m}}$ (m) are the canopy roughness lengths for heat and momentum, ψ_m and ψ_h are unit less functions to correct for atmospheric stability following Högstrom (1996) and Beljaars and Holtslag (1991). In addition to Blyth et al. (1999), and following e.g. Koivusalo and Kokkonen (2002), we introduce an additional parameter $c_{\mathrm{h}0}$ ($\mathrm{W\,m^{-2}\,K^{-1}}$) representing a minimum heat exchange coefficient at windless conditions. Displacement height, and canopy surface roughness length of momentum and heat are related to the canopy height through the parameters f_d (–), f_{z0m} (–), and $f_{\mathrm{z0h/z0m}}$ (–) with values reported in Table 1:

$$d = f_\mathrm{d} z_{\mathrm{can}} \tag{29}$$

$$z_{0\mathrm{m}} = f_{\mathrm{z0m}} z_{\mathrm{can}} \tag{30}$$

$$z_{0\mathrm{h}} = f_{\mathrm{z0h/z0m}} z_{0\mathrm{m}} \tag{31}$$

In addition to the resistance between the canopy air (canopy reference level) and the reference level for meteorological measurements above, excess resistances from the canopy surface, and from the soil/snow surface below, to the canopy level are defined as:

$$r_{\mathrm{can}} = \ln\left(\frac{z_{0\mathrm{m}}}{z_{0\mathrm{h}}}\right) \frac{1}{u_* k} \tag{32}$$

$$r_{\mathrm{surf}} = \ln\left(\frac{z_{0\mathrm{m}}}{z_{0\mathrm{h,\,surf}}}\right) \frac{1}{u_* k} f_{\mathrm{surf}} \tag{33}$$

introducing a multiplicative increase of the resistance below the canopy f_{surf} (–) as a function of the leaf area index:

$$f_{\mathrm{surf}} = 1 + r_{\mathrm{a,LAI}} \left(1 - \exp\{-\mathrm{LAI}\}\right) \tag{34}$$

GMDD
8, 209–262, 2015

A two-layer canopy with thermal inertia

I. Gouttevin et al.

with a maximum value of $1+r_{a,LAI}$ (–). The excess surface resistance below the canopy, r_{surf}, affects the heat and latent fluxes computed from the ground to the reference level. This resistance is corrected for atmospheric stability by applying the same stability functions as in Eqs. (27) and (28), but in this case using the temperature difference between the canopy and the snow or bare soil surface instead of the temperature difference between the canopy and the air. With the current choice of parameter values, the excess resistance for the canopy surface is almost zero, but the theoretical framework for a later use/optimization of this parameter based on observational data is set.

In the end, the total aerodynamic resistances for heat from the reference level to the canopy and the ground surface, respectively, are given by:

$$r_{H,can} = r_{air} + r_{can} \tag{35}$$

$$r_{H,surf} = r_{air} + r_{surf} \tag{36}$$

The aerodynamic resistances for sensible and latent heat from the ground surface are assumed to be equal. For evaporation from intercepted snow, the resistance from the canopy to the canopy layer can be increased with a factor $f_{ra,\,snow}$ (–) compared to rain following Lundberg et al. (1998) and Koivusalo and Kokkonen (2002):

$$r_{Eint} = r_{air} + r_{can} \times \begin{Bmatrix} f_{ra,\,snow}, & T_{air} < 0\,^{\circ}\mathrm{C} \\ 1, & T_{air} \geq 0\,^{\circ}\mathrm{C} \end{Bmatrix} \tag{37}$$

The total resistance for transpiration also takes the stomatal control into account:

$$r_{Etr} = r_{air} + r_{can} + r_{stomata} \tag{38}$$

where the stomata resistance $r_{stomata}$ (–) is calculated as a function of a minimum resistance r_{smin} (–), solar shortwave radiation, vapour pressure deficit and soil water content θ_{soil} as suggested by Jarvis (1976), and soil temperature T_{soil} following Mellander et al. (2006) and Axelsson and Ågren (1976):

$$r_{stomata} = r_{smin}\frac{f_1[\mathrm{SW}_{\downarrow}]f_2[e_{sat}-e_{air}]f_3[\theta_{soil}]f_4[T_{soil}]}{\mathrm{LAI}} \tag{39}$$

GMDD
8, 209–262, 2015
A two-layer canopy with thermal inertia
I. Gouttevin et al.

The functions $f_1 - f_4$ in Eq. (39) all take values between 0 and 1, specifying optimal conditions for root water uptake corresponding to the response of the leaf stomata to conditions in the atmosphere and the root zone.

2.4.4 Biomass heat flux

Due to their thermal inertia, trees can store energy over periods of high exposure to solar radiation, and release it at night. This biomass heat flux is accounted for in the 1LHM version of the canopy module via the areal heat mass of trees $\mathrm{HM_{can}}$ ($\mathrm{J\,K^{-1}\,m^{-2}}$):

$$\mathrm{BM_{can}} = \mathrm{HM_{can}} \cdot \frac{T_{\mathrm{can}}^{t} - T_{\mathrm{can}}^{t-1}}{\Delta t} \quad (40)$$

where T_{can}^{t} (K) and T_{can}^{t-1} are the canopy temperature at the model t and $t-1$ timesteps, and Δt (s) is the model timestep. $\mathrm{HM_{can}}$ is here derived from parameters commonly observed by foresters: LAI, mean stand basal area B ($\mathrm{m^2\,m^{-2}}$) and mean canopy height (z_{can}).

$$\mathrm{HM_{can}} = \mathrm{HM_{leaves}} + \mathrm{HM_{trunk}} \quad (41)$$

$$\mathrm{HM_{leaves}} = \mathrm{LAI} \times e_{\mathrm{leaf}} \rho_{\mathrm{biomass}} c_{p_{\mathrm{biomass}}} \quad (42)$$

$$\mathrm{HM_{trunk}} = 0.5 \times B z_{\mathrm{can}} \rho_{\mathrm{biomass}} c_{p_{\mathrm{biomass}}} \quad (43)$$

The leaf thickness e_{leaf} (m), biomass density ρ_{biomass} ($\mathrm{kg\,m^{-3}}$) and biomass specific heat mass $c_{p_{\mathrm{biomass}}}$ ($\mathrm{J\,kg^{-1}\,K^{-1}}$) are fixed parameters with values 10^{-3}, 900 and 2800 respectively (Lindroth et al., 2010). In Eq. (43), the volume of woody biomass (referred to as "*trunk*" but comprising trunks and branches assimilated to the innermost canopy layer) is calculated from mean tree basal area and height assuming a conical profile for trunks. In this study, areal heat masses will be expressed as "water equivalent areal heat masses" $\mathrm{HM_{eq}}$ ($\mathrm{kg\,m^{-2}}$), e.g. as the areal mass of water yielding the same heat mass than HM ($\mathrm{J\,K^{-1}\,m^{-2}}$):

$$\mathrm{HM_{eq}} = \frac{\mathrm{HM}}{c_{p_\mathrm{water}}} \tag{44}$$

where $c_{p_\mathrm{water}} = 4181\,\mathrm{J\,kg^{-1}\,K^{-1}}$ is the liquid water specific heat mass.

2.5 Two-layer canopy version

With respect to the 1-layer canopy module, the 2-layer formulation induces changes in the formulation of radiative transfer, turbulent and biomass fluxes, and in the end the energy balance of the canopy. These differences are the focus of the present paragraph, whereby the outer canopy layer is equivalently referred to as *"leaves"* while the inner canopy layer is labelled *"trunk"*. The formulation of the radiative and turbulent components of the 2-layer module is illustrated in Fig. 1.

2.5.1 Radiative transfer

In a real forest the trunk layer intercepts parts of the shortwave and longwave radiation transmitted, reflected and emitted by the uppermost canopy layer and upwelling from the soil surface.

Our model features a simplified representation of this:

– For SW radiations, only the transmitted radiations from the upper canopy (with absorption factor σ_fleaves and albedo α_leaves) are intercepted or reflected by the trunk layer (with the respective factors σ_ftrunk and α_trunk). Radiations undergoing multiple reflections between ground surface and upper canopy are unaffected by the trunk layer (Fig. 1). The SW flux reaching the ground and both canopy layers are expressed accordingly:

$$\mathrm{SW_{net,\,trunk}} = \mathrm{SW}_\downarrow(1-\sigma_\mathrm{fleaves})(1-\alpha_\mathrm{trunk})\sigma_\mathrm{ftrunk} \tag{45}$$

Discussion Paper | Discussion Paper | Discussion Paper | Discussion Paper |
GMDD
8, 209–262, 2015
A two-layer canopy with thermal inertia
I. Gouttevin et al.
Title Page
Abstract Introduction
Conclusions References
Tables Figures
Back Close
Full Screen / Esc
Printer-friendly Version
Interactive Discussion

$$\mathrm{SW}_{\text{net, leaves}} = \mathrm{SW}_{\downarrow}(1-\alpha_{\text{leaves}})\sigma_{\text{fleaves}}\left(1+\frac{\alpha_{\text{surf}}(1-\sigma_{\text{fleaves}})(1-\sigma_{\text{ftrunk}})}{1-\sigma_{\text{fleaves}}\alpha_{\text{surf}}\alpha_{\text{trunk}}}\right) \tag{46}$$

$$\mathrm{SW}_{\text{net, surf, 2L}} = \mathrm{SW}_{\downarrow}\frac{(1-\sigma_{\text{fleaves}})(1-\sigma_{\text{ftrunk}})(1-\alpha_{\text{surf}})}{1-\sigma_{\text{fleaves}}\alpha_{\text{surf}}\alpha_{\text{leaves}}} \tag{47}$$

Obviously, the biomass responsible for SW and LW extinction has now to be split into the two canopy layers so that the total extinction for SW is similar in both versions. Equating the first order radiations from Eqs. (11) and (47) yields:

$$(1-\sigma_{\text{f}}) = (1-\sigma_{\text{fleaves}})(1-\sigma_{\text{ftrunk}}) \tag{48}$$

Or equivalently, based on Eq. (17):

$$\mathrm{LAI} = \mathrm{LAI}_{\text{leaves}} + \mathrm{LAI}_{\text{trunk}} \tag{49}$$

where $\mathrm{LAI}_{\text{leaves}}$ and $\mathrm{LAI}_{\text{trunk}}$ are the respective portions of the total LAI attributable to the outer and inner canopies. We denote hereafter

$$f_{\text{LAI}} = \frac{\mathrm{LAI}_{\text{leaves}}}{\mathrm{LAI}} \tag{50}$$

and express the leaves-layer and trunk-layer absorption factors as functions of LAI and f_{LAI}:

$$\sigma_{\text{fleaves}} = 1-\exp\{-k_{\text{LAI}}f_{\text{LAI}}\cdot\mathrm{LAI}\} \tag{51}$$

$$\sigma_{\text{ftrunk}} = 1-\exp\{-k_{\text{LAI}}(1-f_{\text{LAI}})\cdot\mathrm{LAI}\} \tag{52}$$

Similarly to the 1-layer version (Eq. 18), these factors can be adapted to enhance absorption of direct SW radiations based on solar elevation angle.

f_{LAI} is an a priori undetermined parameter of our model due to the difficulty of deriving it from of existing datasets for different forest types and structures. In Sect. 4, the calibration of the model at Alptal against this parameter yields $f_{\text{LAI}} = 0.5$, which means equal contribution from the woody and leafy parts of the forest to shortwave extinctions, and which is kept as default value in the model (see Sect. 5 for discussion).

– For LW radiations, the choice of an emissivity of 1.0 for ground and canopy suppresses multiple reflections. Thermal emissions from the outermost canopy layer and from the ground are attenuated by the trunk layer with the same absorption factor as for SW radiations σ_{ftrunk}. The trunk layer then radiates thermally towards the ground and the outermost canopy layer and sky.

$$\mathrm{LW}_{\text{net, trunk}} = \sigma_{\text{ftrunk}}\left(\mathrm{LW}_{\downarrow}(1-\sigma_{\text{fleaves}}) + \sigma T_{\text{surf}}^4 + \sigma_{\text{fleaves}}\sigma T_{\text{leaves}}^4 - 2\sigma T_{\text{trunk}}^4\right) \tag{53}$$

$$\mathrm{LW}_{\text{net, leaves}} = \sigma_{\text{fleaves}}\left(\mathrm{LW}_{\downarrow} + \sigma T_{\text{surf}}^4(1-\sigma_{\text{ftrunk}}) + \sigma_{\text{ftrunk}}\sigma T_{\text{trunk}}^4 - 2\sigma T_{\text{leaves}}^4\right) \tag{54}$$

$$\begin{aligned}\mathrm{LW}_{\text{net, surf, 2L}} = {} & (1-\sigma_{\text{fleaves}})(1-\sigma_{\text{ftrunk}})\mathrm{LW}_{\downarrow} + \sigma_{\text{fleaves}}(1-\sigma_{\text{ftrunk}})\sigma T_{\text{leaves}}^4 \\ & + \sigma_{\text{ftrunk}}\sigma T_{\text{trunk}}^4 - \sigma T_{\text{surf}}^4\end{aligned} \tag{55}$$

As for the 1-layer version, this radiation balance is only valid on the canopy-covered fraction of the model grid-cell, which is $(1-c_{\text{f}})$ for diffuse SW radiations and LW radiations, and $(1-c_{\text{f, dir}})$ for direct SW.

2.5.2 Turbulent fluxes

Sensible heat exchange between the innermost or outermost canopy layer and the atmosphere is parameterized the same way as in the one-layer model version, e.g. via the resistance $r_{\text{H, can}}$. We consider that latent heat exchange between canopy and atmosphere only occurs through interception evaporation and transpiration at the leaf-level, e.g. via the outermost canopy layer only.

2.5.3 Biomass heat flux

The outer and inner canopy layers are respectively attributed the $\mathrm{HM}_{\text{leaves}}$ and $\mathrm{HM}_{\text{trunk}}$ heat masses from Eqs. (42) and (43), which are used in the biomass heat flux parameterization (Eq. 40) in the place of HM_{can}.

2.5.4 Energy balance

An energy balance is formulated separately for each layer according to the energy balance equation with heat mass (Eq. 8), where all terms are linearized as functions of T_{leaves} and T_{trunk}. The coupled system is then iteratively solved for both temperatures.

The values of all the model parameters as used in the SNOWPACK canopy module are listed in Table 1.

3 Data and methods

3.1 Data

The data from two field sites are used here.

3.1.1 Alptal site

The first data set is from the Alptal forest site (47°03′ N, 8°43′ E, Switzerland) that served as test-site for the SNOWMIP intercomparison study (Rutter et al., 2009) and builds on a long tradition of snow and meteorological investigations (e.g. Stähli et al., 2006, 2009).

The site is more exactly located in the Erlenbach sub-catchment of the Alptal valley, with an ~11° west-orientated slope at 1185 m a.s.l. (site 1012 in the Fig. 1 of Stähli et al., 2006). The stand is dominated by Norway spruce (85 %) and silver fir (15 %), with a basal area of 41 $m^2\,ha^{-1}$ and a maximum height of typically 25 m. The site LAI (including slope corrections and corrections for clumping) ranges from 3.41 to 4.57 with mean value of 3.9 $m^2\,m^{-2}$ (Stähli et al., 2009).

At this site, the SNOWPACK model is run using meteorological data derived from observations:

GMDD
8, 209–262, 2015

- Downward shortwave and longwave radiation measured on a 35 m-high mast above the canopy forest. The instrument is a heated, non-ventilated CNR1 from Kipp and Zonen (2002) comprising two pyranometers CM3 (for SW) and two pyrgeometers CG3 (for LW).
- Precipitations measured by a heated gauge placed at 25 m height on the high mast, so that the highest trees provide a sheltering similar to a fence.
- Wind speed recorded by a cup anemometer (WMS) at 35 m on the mast.
- Air temperature measured at 35 m by a ventilated thermo-hygrometer Thygan (Meteolabor) also integrating a dew point hygrometer.
- Relative air humidity at 35 m height, derived from the air temperature and dew point.

Validation data include:

- Downward SW and LW radiations measured below the canopy ($LW{\downarrow}_{BC}$, $SW{\downarrow}_{BC}$) by a second CNR1 radiation sensor as described above, but mounted on a carrier constantly moving along a 10 m-long transect at 2 m altitude above ground at 1 m min^{-1} speed. This transect was previously shown to have a representative LAI for the stand (Stähli et al., 2009). Great care was put in the collection and pre-processing of this dataset, as below-canopy SW radiation is typically close to zero. This effort is well described in Stähli et al. (2009).

  As a post-treatment to this dataset, the LW radiation data were masked in cases when snow interception on the sensor was suspected. A typical such case is illustrated in Fig. 2: from the evening of 19 to 21 February at midday, the heated pyrgeometer measures radiations close to the emissions of a blackbody at 0 °C (snow emissivity is around 0.98), whereas the air temperature is much colder and modelled canopy temperature closely follows the air temperature signal. The precipitation record (Fig. 2b) features almost continuous snowfall over that period. It

GMDD
8, 209–262, 2015

is hence suspected that the measured radiations originate from snow at temperature close to 0 °C covering the heated pyrgeometer, and not from LW emissions by the canopy. Due to their flat geometry, upwards-looking pyrgeometers are likely to remain covered by snow for substantial periods, typically a few days in alpine temperate winters. Over the 2003–2007 period, an average of 25 days per year were masked after visual identification of such events.

– Snow depth, snow density and snow water equivalent (SWE) that were measured below the canopy on a weekly basis, at 1 m intervals along a 30 m transect adjacent to the trajectory of the radiometer-carrier. More details of the exact procedure are available in Stähli et al. (2009). We use the spatial average of the measurements to come up with stand-representative values.

Meteorological and validation data are available for four consecutive winter seasons between 2003 and 2007.

3.1.2 Norunda site

The second dataset is from the Norunda forest site (60°05′ N, 17°28′ E), located in a quite level region about 30 km north of Uppsala, Sweden, at 45 m a.s.l. Since June 1994 it is equipped with meteorological instruments, which were complemented by biomass thermometers in June and July 1995. The forest stand is composed of Scots pine (61 %), Norway spruce (34 %) and birch (5 %) with a stand LAI comprised between 4 and 5 $m^2 m^{-2}$, a mean basal area of ~ 34.7 $m^2 ha^{-1}$, and a maximum tree height of ~ 28 m.

At this site, SNOWPACK is driven by observed meteorological variables:

– Downwelling LW and SW radiation measured by a combination of a ventilated CM21 pyranometer (Kipp and Zonen) placed at 102 m above ground and a ventilated LXV055 net radiometer at 68 m above ground.

GMDD
8, 209–262, 2015
A two-layer canopy with thermal inertia
I. Gouttevin et al.

- Air temperature recorded at 37 m height above ground by a copper-constantan thermocouple placed in the ventilated radiation shields.
- Air humidity measured at 28 m by a HP100 TST probe (Robotronic).
- Wind speed recorded at 37 m by a sonic anemometer.
- Precipitation data were unfortunately not available at the site. We therefore made use of precipitation data recorded at the Uppsala Aut WMO-station (WMO number: 2–462. This station is 26 km away from the Norunda site and the nearest operating in summer 1995) openly provided by the Swedish Meteorological and Hydrological Institute (SMHI, http://opendata-catalog.smhi.se/explore/).

The specificity of the Norunda site lies in the continuous measurement, over a summer, of the biomass temperature at different heights and depths within the trunks and branches of the dominant tree species: pines and spruces. They were complemented by a detailed calculation of tree-level and stand-level biomass heat storage, which builds a unique dataset to evaluate a physics-based canopy model with heat-mass. The details of the tree temperature measurements and heat storage calculations can be found in Lindroth et al. (2010).

In the present study we make use pine trunk temperature at 1.5 m height, which have been measured close to the trunk surface (1 cm deep within the bark). Indeed, we are mostly interested in the ability of the model to reproduce the trunk surface temperature, which generate the thermal emissions of the trunk layer. We also provide an assessment of the canopy energy balance modelled by SNOWPACK by comparing the stand-scale modelled biomass storage flux to the one inferred from observations by Lindroth et al. (2010).

3.2 Methods: model calibration

Three versions of the canopy module, corresponding to activation of the different features of the new developments (bi-layered canopy and heat mass, Table 2), are calibrated at Alptal in order to evaluate the model in its best-performance set-up. Calibration is performed against the observed incoming longwave and shortwave radiation below the canopy ($LW{\downarrow}_{BC}$, $SW{\downarrow}_{BC}$), which are specifically affected by the new developments. The observed sub-canopy SWE is not used for calibration because of uncertainties related to the snowpack modelling that could potentially compromise a proper calibration of the canopy module.

Depending on the version, one or two model parameters are calibrated, consistently with our modelling choices: k_{LAI} and/or f_{LAI} (Table 2).

Canopy heat mass also affects the LW radiations down-welling to the ground surface. Heat mass is a physical property of a forest stand, and not a free parameter of the model. However, its value is difficult to measure and our model only proposes a coarse estimation of it (see Sect. 2). In each of the versions with heat mass, we therefore try to optimize its value considering it as an additional calibration parameter (versions 1LHM* and 2LHM*, Table 2). This procedure is designed to assess the physical consistency of our formulation, by comparing its performance to results obtained with unrealistic heat mass values.

Calibration is performed by minimizing the error function CC, which is the sum of the model-to-data RMSE (Root Mean Square Error) and MB (Mean Bias) for the two observed variables $LW{\downarrow}_{BC}$, $SW{\downarrow}_{BC}$.

$$CC = |MB(LW{\downarrow}_{BC})| + |MB(SW{\downarrow}_{BC})| + RMSE(LW{\downarrow}_{BC}) + RMSE(SW{\downarrow}_{BC})$$

We prefer CC over the more common Nash–Sutcliff efficiency (NSE) because $LW{\downarrow}_{BC}$ and $SW{\downarrow}_{BC}$ exhibit a strong diurnal cycle: for such cyclic variables, even a low-performance representation of the cycles yields a high NSE, and the NSE sensitivity to further improvements is typically low (Schaefli and Gupta, 2007).

GMDD
8, 209–262, 2015

4 Results

4.1 Alptal

4.1.1 Model calibration

Table 3 summarizes the results of the calibration of the five model versions (1LnoHM, 1LHM, 2LHM, 1LHM*, 2LHM*) against $LW{\downarrow}_{BC}$ and $SW{\downarrow}_{BC}$ data from the snow season 2003–2004.

For all versions, the calibrated extinction coefficient k_{LAI} is within the [0.4–0.8] range of expected values (Stähli et al., 2009). Both $LW{\downarrow}_{BC}$ and $SW{\downarrow}_{BC}$ are affected by k_{LAI}, but $LW{\downarrow}_{BC}$ is less sensitive to radiation extinction (as atmospheric LW extinction by canopy is partly compensated by canopy thermal emission in the same range of magnitudes). k_{LAI} is therefore mostly determined by calibration against $SW{\downarrow}_{BC}$ and is the same for most versions, which differ only in their modelling of $LW{\downarrow}_{BC}$.

The calibration of the f_{LAI} parameter partitioning LAI between the uppermost and lowermost canopy layers in the 2LHM version also yields the reasonable value of 0.5: this would have been the natural modelling choice for partitioning the canopy into two layers.

The successive addition of heat mass (1LHM) and a two-layer partition in the canopy (2LHM) to the default 1LnoHM simulation improves the general model performance, as reflected in the decrease of the CC error function and its components (MB, RMSE).

In the two versions where canopy heat mass is optimized (1LHM*, 2LHM*), optimization yields unrealistically high heat mass values (HM = 90 $kg\,m^{-2}$ and HM = 60 $kg\,m^{-2}$ respectively, whereby field data indicate 30 $kg\,m^{-2}$). However, while optimizing heat mass quite significantly improves the performance of the 1-layer versions (from CC = 23.6 $W\,m^{-2}$ for 1LHM to CC = 19.3 $W\,m^{-2}$ for 1LHM*), it only marginally affects the performance of the 2-layer version (from CC = 18.4 $W\,m^{-2}$ for 2LHM to CC = 17.5 $W\,m^{-2}$ for 2LnoHM). These are encouraging results for the 2-layer canopy formulation: on the one hand, this model version shows a better performance than the one-layered canopy

GMDD
8, 209–262, 2015

model, even with the physically-estimated heat mass. Such a performance can only be approached by the one-layered version with an unrealistic canopy heat mass. On the other hand, the performance of 2LHM show a considerably reduced sensitivity to the prescribed areal heat mass of canopy, a physical parameter which can be spatially variable and hard to retrieve with precision over non-investigated forested areas.

The performance of all model versions after calibration over 2003–2004 slightly degrades over the longer 2003–2007 time-period when observations are available. Especially the MB in $LW\downarrow_{BC}$, and (to a smaller degree) in $SW\downarrow_{BC}$, are increased over 2003–2007, questioning the transferability of our 2003–2004 calibration. We therefore calibrate the 1LnoHM, 1LHM and 2LHM versions over the 2003–2007 period and analyse the changes in best-fit parameters and performance (Table 4).

The calibration over 2003–2007 yields a slightly different best-fit parameter value for the extinction coefficient in the 1LHM and 2LHM versions ($k_{LAI} = 0.85$ vs. $k_{LAI} = 0.75$ when calibrated over 2003–2004): this enhanced radiation extinction improves the MB for $SW\downarrow_{BC}$ over the 2003–2007 period, but slightly degrades the results over 2003–2004. The overall picture is however not changed upon this new calibration:

- Over both periods, 2LHM performs better than 1LHM which also performs better than 1LnoHM: this is an indication of the added value of our new parameterizations.

- For all model versions, performance is better over 2003–2004 than over the full 2003–2007 period, especially for $LW\downarrow_{BC}$. This may indicate that our model is still too simple to capture the full range of snow-forest processes.

- Over both periods, the two, slightly different calibrations yield thoroughly comparable model performances. This gives confidence in the validity of our calibration and in the possibility of calibrating the model over only one year of data.

In the simulations discussed in the rest of the paper, calibration over 2003–2007 is used.

GMDD
8, 209–262, 2015

4.1.2 Model evaluation against thermal radiation

Figure 3 compares observed and modelled $LW{\downarrow}_{BC}$ as computed by the different model versions without heat mass optimization (1LnoHM, 1LHM, 2LHM) over the 2003–2004 calibration period. Similarly to the performance metrics of Table 3, it illustrates gradually increasing model performances from the 1LnoHM to the 2LHM model versions.

With respect to 1LnoHM, the consideration of the trees heat mass in 1LHM slightly delays and reduces the canopy cooling at night and warming up in the morning: this translates into a slight delay and smoothing of the diurnal cycle of $LW{\downarrow}_{BC}$, part of which originate from canopy thermal emissions.

More striking is, however, the attenuation of the daily amplitude of $LW{\downarrow}_{BC}$ induced by 2LHM, which brings the modelling results in closer agreement to observations: especially, the night-time (6PM-6AM) mean bias in $LW{\downarrow}_{BC}$ is considerably reduced in 2LHM with respect to other model versions, amounting to −10.8, −7.8 and $-2.8\,\mathrm{W\,m^{-2}}$ in 1LnoHM, 1LHm and 2LHM respectively.

When only one bulk layer of canopy is considered, this layer is exposed at night to intense radiative cooling towards the sky, whose thermal emissivity is low. With two layers of canopy, only the uppermost layer experiences this uncompensated cooling. The innermost layer receives thermal radiation from the uppermost layer, which has a higher emissivity than the sky. This thermal sheltering yields higher temperatures and LW emissions at night from the inner canopy towards the ground surface. This mechanism proves to efficiently reproduce the daily cycles (Fig. 3a and b) and daily averages (Fig. 3c) of the thermal radiations delivered to the snowpack.

4.1.3 Impact on the underlying snowpack

SWE is the most important variable in snow hydrology. However, as underlined in the Introduction, snowpack modelling is a highly challenging task because untrustworthy inputs (mixed precipitation, snowfall amount) are fed into imperfect models (our attempt here at improving the energy balance in forested context should not conceal that modelled interception and unload do not always reflect ground truth), which additionally accumulate errors in SWE over the snow season. Specifically, Rutter et al. (2009) highlighted that precipitation phase, rain-on-snow events and the treatment of subsequent meltwater by the models, is an area of key sensitivity with respect to SWE modelling. These aspects are not improved by the new canopy module presented here. Therefore, the modelled SWE featured by our three model versions (Figs. 3d and 4) is affected by these uncertainties, which can typically be of the order of magnitude of the inter-model differences in SWE (1 to 5 cm) and preclude an absolute assessment of the superiority of one version over the others. Mixed precipitation events are typically very frequent at Alptal, as illustrated by grey bands on our SWE plots (Figs. 3d and 4). Yet, the investigation of the behavior of our three model versions with respect to observations helps capture the full scope of the changes induced by the new parameterizations. Punctually, it also allows some insight in the improvements induced by the new developments.

Over the four winters of interest here, a similar ranking of sub-canopy SWE modelled by 1LnoHM, 1LHM and 2LHM is observed, with 1LHM accumulating most snow and 2LHM generally featuring the smallest SWE (except for the 2005–2006 winter). With respect to the thermal behaviors associated with the different model versions, such a result is somehow counter-intuitive as 1LHM and 2LHM generally deliver greater amounts of LW radiation to the snowpack, than does 1LnoHM (Fig. 3c), hence contributing more strongly to mid-winter ablation events (e.g. Fig. 3d, December to January). In 1LHM, this increased ablation is, however, compensated by a different effect of the thermal canopy mass: as a result of the high thermal mass of the bulk canopy in 1LHM, the canopy temperature and hence interception evaporation are reduced, and more snow unloads than in the two other versions, resulting in higher sub-canopy snow accumulation. In 2LHM, the high diurnal temperature variations of the outer canopy temperature combine with stronger LW radiation to the snowpack, to build a thinner snowpack.

Noteworthy is that the model ability to represent SWE (as typically assessed by the RMSE to observations) is degraded in 1LHM and improved in 2LHM with respect to the original canopy module, 1LnoHM. The LW-enhanced ablation in 2LHM (and small as-

GMDD
8, 209–262, 2015

sociated changes in interception evaporation) does therefore not deteriorate the overall model skills.

In some specific ablation periods, 2LHM even proves to reproduce the observed snowpack dynamics better: one such event is the early February 2004 severe ablation, when high thermal exposure of the snowpack is better reproduced by 2LHM (Fig. 3c) while the concomitant ablation is also stronger in 2LHM, which matches the observations better (Fig. 3d). Similarly, the LW-enhanced ablation in 2LHM leads to a sub-canopy SWE dynamics in closer agreement with observations in the 2005 ablation phase and in early 2007 (mid-winter complete snow disappearance). These are encouraging results for the overall consistency of the canopy module.

4.2 Norunda: tree temperature and biomass storage flux

At the Norunda site, SNOWPACK is run using the Alptal calibration from 2003–2007, and a canopy basal area and areal heat mass derived from local data (Sect. 3). The difference in latitudes (hence in solar angle), tree species (mostly Scots Pine at Norunda) and context (Alpine winter vs. boreal summer) between both sites constitutes a huge challenge and an excellent benchmark to test one desired feature of a physically-based model, e.g. its transferability to different climate and ecosystem types.

We compare observed tree trunk temperatures to modelled temperatures of the bulk canopy (for 1LnoHM and 1LHM) or of the lower trunk layer (for 2LHM) over summer 1995 at Norunda (Fig. 5, Table 5). The modelled trunk layer temperature of 2LHM shows an improved ability to reproduce the observed tree trunk temperature signal: similiar to the improvements seen at Alptal, 2LHM considerably reduces the radiative loss of the lowermost canopy at night, bringing night-time modelled temperatures in closer agreement to observed data at Norunda. Also, the reduced SW insolation received by the lower canopy layer during daytime in 2LHM prevents too high mid-day temperatures for the trunks, an observation that 1LHM and 1LnoHM cannot reproduce. Finally, the combination of thermal sheltering of the lowermost canopy layer and its thermal inertia delays the tree trunk cooling (resp. warming) at evening (resp. morning) times, improving the temporal correlation with observations.

Heat fluxes to canopy elements are a substantial, though not dominant, component of the canopy energy balance (Lindroth et al., 2010, their Fig. 6): they can amount to ~ 7 % of the daily net radiation received by the canopy. To assess the consistency of the SNOWPACK canopy module we compare the modelled canopy heat fluxes to the ones derived by Lindroth et al. from field measurements and extrapolated at the stand scale. Note that 1LnoHM, having no heat mass, does not model any such fluxes.

Both 1LHM and 2LHM versions overestimate the daily amplitude of biomass heat fluxes with respect to observations, with an increased bias for 1LHM (Fig. 6; Table 5). This is in line with an overestimation of the daily amplitude of canopy or lower canopy-layer temperatures (Fig. 5), which is stronger for 1LHM. Also, the model biomass heat fluxes peak ~ 2 h earlier than the observed ones. This is an artefact of modelling the canopy as a continuous wooden material layer, where thermal diffusion occurs, with only one or two thermally homogeneous layers. In reality, the low thermal inertia of a bark surface layer provokes quick surface heating and temporarily limits further heating from turbulent and radiative fluxes. Contrarily, a bulk, thermally inert layer heats up to a smaller temperature which allows for further sustained heating. As a result, our modelled canopy reacts more rapidly than a real one to the diurnal heating cycle.

As such, the representation of the biomass storage fluxes by 1LHM and 2LHM yield only moderate improvement to the model: they feature a reasonable (though slightly shifted) diurnal cycle (cf. the correlation coefficients in Table 5) but their RMSE to observations is of the order of magnitude of the SD of the observed biomass fluxes (Table 5, first row).

However, model performance, especially for 2LHM, is improved if the total heat storage flux towards the biomass and canopy air space is considered (thick black line in Fig. 6, Table 5). The air heat storage flux corresponds to the changes in latent and sensible heat stored in the within-canopy air space. Lindroth et al. (2010) provide estimates of these heat storage terms based on air temperature and humidity measurements at

7 heights within the canopy air space. On a daily basis, the air heat storage term reacts more rapidly to solar heating than the biomass heat storage flux. The air heat storage flux is not specifically accounted for in SNOWPACK. However, the increased correlation coefficient and reduced RMSE obtained when the SNOWPACK canopy heat flux is compared to the sum of estimated air and biomass heat fluxes, indicate that the canopy module produces a bulk representation of the observed fluxes. This may be the result of error compensations, the simple 2-layer scheme with no heat diffusion inside bulkly mimicking a system where air takes up heat rapidly while biomass heats up more slowly. Such a result should be confirmed against further observational datasets.

5 Discussion

Our results show that the new features implemented in the SNOWPACK canopy module, especially the two-layer canopy, improve the representation of the radiation budget at the sub-canopy level. The importance of assessing the temperature contrasts between different canopy elements has often been underlined (Sicart et al., 2004; Pomeroy et al., 2009), but the validation of this hypothesis with a seamless physics-based canopy model had never been brought to the scientific literature. As radiations are one of the main drivers of the spring-time sub-canopy snow energy balance (e.g. Garvelmann et al., 2014), this constitutes an important achievement.

Other processes, which lead to input of melt energy, such as mixed-precipitation or rain-on-snow events, interact with the radiation transfer. A robust representation of canopy radiative transfer at the stand scale can help pinpoint, constrain and correct model shortcomings related to these other critical processes.

Further wintertime assessment of model performance in colder environments, where mixed precipitation events are scarce, would for instance provide an excellent test-case to confirm the added value of our new canopy formulation for the representation of sub-canopy snow dynamics, and better constrain our representation of e.g. turbulent fluxes.

GMDD
8, 209–262, 2015

SNOWPACK has a multi-layer and detailed representation of snow and soil, which features a highly resolved modelling of energy and mass balance in thin layers including e.g. snow metamorphism and freezing point depressions during phase change in soil (Wever et al., 2014). This detailed and physics-based description should have a corresponding representation of canopy processes, which has not been the case in earlier versions of SNOWPACK. The more detailed model described in this contribution is therefore a consistent extension of SNOWPACK and leads to an overall more balanced representation of processes in the air–vegetation–snow–soil continuum.

The two-layer formulation furthermore builds a suitable basis for a future model adaptation to deciduous forest environments.

This formulation exhibits robustness in two ways:

- First, it shows little sensitivity to physical parameters that are hard to assess from standard forestry metrics or for non-investigated forests. The canopy heat mass is one of such parameters, as stated in Sect. 4. The other one is the fraction of LAI attributed to the top-most ("leafy") canopy layer, as illustrated in Fig. 7. The ratio of woody to total plant area is hard to measure optically, especially for evergreen canopies (Weiss et al., 2004). Pomeroy et al. (2009) used a formulation somewhat similar to ours to attribute LW radiations to emissions from leafy or woody elements. They conclude that, depending on the forest structure and type, the needle-branch fraction as seen from a ground observer would range from 0.6 to 0.75 of the total plant elements. Our Alptal calibration attributing 50 % of canopy LAI to the uppermost, leaf-only layer is consistent with this model-based estimate for leaf and branches elements.

- Second, the model exhibits a good performance at the Norunda site, while its free parameters (k_{LAI} and f_{LAI}) have been calibrated in a different forest ecosystem and climatic context at Alptal. In both forests, coniferous species are dominant and it is suspected that extrapolation of our parameterizations to deciduous forests requires further adaptation. However, this result gives confidence in the possibility

GMDD
8, 209–262, 2015

of using our physics-based model without prior tuning in different alpine and subarctic catchments majorly covered by conifers.

Finally, it is a quite general finding that two-layer formulations often bring substantial improvements over single-layer ones. The step from the big-leaf soil-vegetation-atmosphere transfer models to the dual-source models (e.g. Blyth et al., 1999; Bewley et al., 2010) is a typically illustration of this phenomenon for the computation of the land surface energy balance. In a domain more closely related to canopies, Dai et al. (2004) improved their modelling of forest CO_2 absorption by considering different regimes for sunlit and shaded leaves. Our results here are in line with this more general observation.

6 Conclusions

Our new canopy model demonstrates ability to simulate the difference in the thermal regimes of the canopy leafy and woody compartments, as assessed by comparison to observed canopy temperatures and thermal emissions. This is achieved via the separation of the canopy in two layers of different heat masses, radiatively interacting with each-other. In comparison, a one-layered version of the canopy module always yields poorer results despite optimization attempts. The most striking improvement is the reduction in night-time canopy cold bias, which can only be achieved via the two-layer formulation and results from the sheltering role of the upper canopy layer.

The robustness of the new canopy model is confirmed by the successful evaluation of the model without prior tuning at a boreal, coniferous site. The new formulation besides shows a weak sensitivity to biomass areal heat mass, a forest-dependent input parameter that can be hard to estimate locally. Model evaluation against snow water equivalent data indicate that the new parameterization do not degrade the overall model skills while improving the representation of some LW-enhanced ablation events.

GMDD
8, 209–262, 2015
A two-layer canopy with thermal inertia
I. Gouttevin et al.

The improved representation of the radiative components of the sub-canopy energy balance achieved here opens the path to the tracking, understanding and modelling of further processes relevant for the underlying snowpack like turbulent fluxes or heat advection by rain.

Acknowledgements. We thank the CRYOS team and IRSTEA for the funding of a one-year and a half visiting scientist position at EPFL.

References

ACIA: Arctic Climate Impact Assessment, Cambridge University Press, available at: http://www.acia.uaf.edu (last access: September 2010), 2005.

Adams, R., Spittlehouse, D., and Winkler, R.: The effect of a canopy on the snowmelt energy balance, in: Proceedings of the 64th Annual Western Snow Conference, Bend, Oregon, 171–174, 1996.

Axelsson, B. and Agren, G.: Tree Growth Model (PT 1) a Development Paper, Swedish Coniferous Forest Project Internal Report, Uppsala, 1976.

Bartelt, P. and Lehning, M.: A physical SNOWPACK model for the Swiss avalanche warning: Part I: numerical model, Cold Reg. Sci. Technol., 35, 123–145, 2002.

Beljaars, A. and Holtslag, A.: Flux parameterization over land surfaces for atmospheric models, J. Appl. Meteorol., 30, 327–341, 1991.

Bewley, D., Essery, R., Pomeroy, J., and Ménard, C.: Measurements and modelling of snowmelt and turbulent heat fluxes over shrub tundra, Hydrol. Earth Syst. Sci., 14, 1331–1340, doi:10.5194/hess-14-1331-2010, 2010.

Blyth, E. M., Harding, R. J., and Essery, R.: A coupled dual source GCM SVAT, Hydrol. Earth Syst. Sci., 3, 71–84, doi:10.5194/hess-3-71-1999, 1999.

Chen, J. M., Rich, P. M., Gower, S. T., Norman, J. M., and Plummer, S.: Leaf area index of boreal forests: theory, techniques, and measurements, J. Geophys. Res.-Atmos., 102, 29429–29443, 1997.

Dai, Y., Dickinson, R. E., and Wang, Y.-P.: A two-big-leaf model for canopy temperature, photosynthesis, and stomatal conductance, J. Climate, 17, 2281–2299, 2004.

GMDD
8, 209–262, 2015

Erbs, D., Klein, S., and Duffie, J.: Estimation of the diffuse radiation fraction for hourly, daily and monthly-average global radiation, Sol. Energy, 28, 293–302, 1982.
Essery, R., Li, L., and Pomeroy, J.: A distributed model of blowing snow over complex terrain, Hydrol. Process., 13, 2423–2438, 1999.
Essery, R., Pomeroy, J., Parviainen, J., and Storck, P.: Sublimation of snow from coniferous forests in a climate model, J. Climate, 16, 1855–1864, 2003.
Essery, R., Rutter, N., Pomeroy, J., Baxter, R., Stahli, M., Gustafsson, D., Barr, A., Bartlett, P., and Elder, K.: SnowMIP2: an evaluation of forest snow process simulation, B. Am. Meteorol. Soc., 90, 1120–1135, doi:10.1175/2009BAMS2629.1, 2008.
Garvelmann, J., Pohl, S., and Weiler, M.: Variability of observed energy fluxes during rain-on-snow and clear sky snowmelt in a mid-latitude mountain environment, J. Hydrometeorol., 15, 1220–1237, doi:10.1175/JHM-D-13-0187.1, 2014.
Gouttevin, I., Menegoz, M., Dominé, F., Krinner, G., Koven, C., Ciais, P., Tarnocai, C., and Boike, J.: How the insulating properties of snow affect soil carbon distribution in the continental pan-Arctic area, J. Geophys. Res., 117, G02020, doi:10.1029/2011JG001916, 2012.
Grippa, M., Kergoat, L., Le Toan, T., Mognard, N., Delbart, N., L'Hermitte, J., and Vicente-Serrano, S.: The impact of snow depth and snowmelt on the vegetation variability over central Siberia, Geophys. Res. Lett., 32, L21412, doi:10.1029/2005GL024286, 2005.
Gryning, S.-E., Batchvarova, E., and De Bruin, H.: Energy balance of a sparse coniferous high-latitude forest under winter conditions, Bound.-Lay. Meteorol., 99, 465–488, 2001.
Gustafsson, J., Brooks, P., Molotch, N., and Veatch, W.: Estimating snow sublimation using natural chemical and isotopic tracers across a gradient of solar radiation, Water Resour. Res., 46, W12511, doi:10.1029/2009WR009060, 2010.
Harding, R. and Pomeroy, J.: The energy balance of the winter boreal landscape, J. Climate, 9, 2778–2787, 1996.
Hardy, J., Davis, R., Jordan, R., Li, X., Woodcock, C., Ni, W., and McKenzie, J.: Snow ablation modeling at the stand scale in a boreal jack pine forest, J. Geophys. Res.-Atmos., 102, 29397–29405, 1997.
Hedstrom, N. and Pomeroy, J.: Measurements and modelling of snow interception in the boreal forest, Hydrol. Process., 12, 1611–1625, 1998.
Helbig, N., Löwe, H., and Lehning, M.: Radiosity approach for the shortwave surface radiation balance in complex terrain, J. Atmospheric Sci., 66, 2900–2912, 2009.

GMDD
8, 209–262, 2015
A two-layer canopy with thermal inertia
I. Gouttevin et al.

Hogstrom, U.: Review of some basic characteristics of the atmospheric surface layer, Bound.-Lay. Meteorol. 25th Anniversary Volume, 215–246, 1996.
Jansson, P. and Karlberg, L.: Coupled Heat and Mass Transfer Model For Soil–Plant–Atmosphere Systems, TRITA-AMI report 30 87, Royal Institute of Technology, Department of Civil and Environmental Engineering, Stockholm, 435 pp., 2001.
Jarvis, P.: The interpretation of the variations in leaf water potential and stomatal conductance found in canopies in the field, Philos. T. R. Soc. Lond., 273, 593–610, 1976.
Kavetski, D. and Kuczera, G.: Model smoothing strategies to remove microscale discontinuities and spurious secondary optima in objective functions in hydrological calibration, Water Resour. Res., 43, W03411, doi:10.1029/2006WR005195, 2007.
Kelley Jr, J., Weaver, D., and Smith, B.: The variation of carbon dioxide under the snow in the Arctic, Ecol., 49, 358–361, doi:10.2307/1934472, 1968.
Kipp and Zonen B.V.: Instruction Manual to the CNR1 Net Radiometer, Delft, the Netherlands, Kipp and Zonen B.V., 2002.
Koivusalo, H. and Kokkonen, T.: Snow processes in a forest clearing and in a coniferous forest, J. Hydrol., 262, 145–164, 2002.
Lawrence, D. and Slater, A.: The contribution of snow condition trends to future ground climate, Clim. Dynam., 34, 969–981, 2010.
Lehning, M., Bartelt, P., Brown, B., and Fierz, C.: A physical SNOWPACK model for the Swiss avalanche warning: Part III: meteorological forcing, thin layer formation and evaluation, Cold Reg. Sci. Technol., 35, 169–184, 2002a.
Lehning, M., Bartelt, P., Brown, B., Fierz, C., and Satyawali, P.: A physical SNOWPACK model for the Swiss avalanche warning: Part II. Snow microstructure, Cold Reg. Sci. Technol., 35, 147–167, 2002b.
Lehning, M., Völksch, I., Gustafsson, D., Nguyen, T. A., Stähli, M., and Zappa, M.: ALPINE3D: a detailed model of mountain surface processes and its application to snow hydrology, Hydrol. Process., 20, 2111–2128, 2006.
Lehning, M., Löwe, H., Ryser, M., and Raderschall, N.: Inhomogeneous precipitation distribution and snow transport in steep terrain, Water Resour. Res., 44, W07404, doi:10.1029/2007WR006545, 2008.
Lindroth, A., Mölder, M., and Lagergren, F.: Heat storage in forest biomass improves energy balance closure, Biogeosciences, 7, 301–313, doi:10.5194/bg-7-301-2010, 2010.

GMDD
8, 209–262, 2015

A two-layer canopy with thermal inertia

I. Gouttevin et al.

Liston, G., Mcfadden, J., Sturm, M., and Pielke, R.: Modelled changes in arctic tundra snow, energy and moisture fluxes due to increased shrubs, Glob. Change Biol., 8, 17–32, 2002.
Lundberg, A., Calder, I., and Harding, R.: Evaporation of intercepted snow: measurement and modelling, J. Hydrol., 206, 151–163, 1998.
Lundquist, J. D., Dickerson-Lange, S. E., Lutz, J. A., and Cristea, N. C.: Lower forest density enhances snow retention in regions with warmer winters: a global framework developed from plot-scale observations and modeling, Water Resour. Res., 49, 6356–6370, 2013.
Mellander, P.-E., Stähli, M., Gustafsson, D., and Bishop, K.: Modelling the effect of low soil temperatures on transpiration by Scots pine, Hydrol. Process., 20, 1929–1944, 2006.
Merriam, R. A.: A note on the interception loss equation, J. Geophys. Res., 65, 3850–3851, 1960.
Musselman, K. N., Molotch, N. P., Margulis, S. A., Lehning, M., and Gustafsson, D.: Improved snowmelt simulations with a canopy model forced with photo-derived direct beam canopy transmissivity, Water Resour. Res., 48, W10509, doi:10.1029/2012WR012285, 2012.
Nash, J. and Sutcliffe, J.: River flow forecasting through conceptual models part IA discussion of principles, J. Hydrol., 10, 282–290, 1970.
Otterman, J., Staenz, K., Itten, K., and Kukla, G.: Dependence of snow melting and surface–atmosphere interactions on the forest structure, Bound.-Lay. Meteorol., 45, 1–8, 1988.
Pomeroy, J. W. and Essery, R.: Turbulent fluxes during blowing snow: field tests of model sublimation predictions, Hydrol. Process., 13, 2963–2975, 1999.
Pomeroy, J. W., Parviainen, J., Hedstrom, N., and Gray, D.: Coupled modelling of forest snow interception and sublimation, Hydrol. Process., 12, 2317–2337, 1998.
Pomeroy, J. W., Gray, D., Hedstrom, N., and Janowicz, J.: Prediction of seasonal snow accumulation in cold climate forests, Hydrol. Process., 16, 3543–3558, 2002.
Pomeroy, J. W., Marks, D., Link, T., Ellis, C., Hardy, J., Rowlands, A., and Granger, R.: The impact of coniferous forest temperature on incoming longwave radiation to melting snow, Hydrol. Process., 23, 2513–2525, 2009.
Rasmus, S., Grönholm, T., Lehning, M., Rasmus, K., and Kulmala, M.: Validation of the SNOWPACK model in five different snow zones in Finland, Boreal Environ. Res., 12, 467–488, 2007.
Rasmus, S., Lundell, R., and Saarinen, T.: Interactions between snow, canopy, and vegetation in a boreal coniferous forest, Plant Ecolology & Diversity, 4, 55–65, 2011.

Rutter, N., Essery, R., Pomeroy, J., Altimir, N., Andreadis, K., Baker, I., Barr, A., Bartlett, P., Boone, A., Deng, H. et al.: Evaluation of forest snow processes models (SnowMIP2), J. Geophys. Res.-Atmos., 114, D06111, doi:10.1029/2008JD011063, 2009.
Saccone, P., Morin, S., Baptist, F., Bonneville, J.-M., Colace, M.-P., Domine, F., Faure, M., Geremia, R., Lochet, J., Poly, F., Lavorel, S., and Clément, J.-C.: The effects of snowpack properties and plant strategies on litter decomposition during winter in subalpine meadows, Plant Soil, 363, 215–229, 2013.
Schaeffli, B. and Gupta, H. V.: Do Nash values have value?, Hydrol. Process., 21, 2075–2080, 2007.
Schmidt, R. and Gluns, D. R.: Snowfall interception on branches of three conifer species, Can. J. Forest Res., 21, 1262–1269, 1991.
Shuttleworth, W. J. and Wallace, J.: Evaporation from sparse crops-an energy combination theory, Q. J. Roy. Meteor. Soc., 111, 839–855, 1985.
Sicart, J. E., Essery, R. L., Pomeroy, J. W., Hardy, J., Link, T., and Marks, D.: A sensitivity study of daytime net radiation during snowmelt to forest canopy and atmospheric conditions, J. Hydrometeorol., 5, 774–784, 2004.
Sivapalan, M., Takeuchi, K., Franks, S., Gupta, V., Karambiri, H., Lakshmi, V., Liang, X., McDonnell, J., Mendiondo, E., O'connell, P., Oki, T., Pomeroy, J. W., Schertzer, D., Uhlenbrook, S., and Zehe, E.: IAHS decade on predictions in ungauged basins (PUB), 2003–2012: shaping an exciting future for the hydrological sciences, Hydrol. Sci. J., 48, 857–880, 2003.
Stähli, M. and Gustafsson, D.: Long-term investigations of the snow cover in a subalpine semi-forested catchment, Hydrol. Process., 20, 411–428, 2006.
Stähli, M., Jonas, T., and Gustafsson, D.: The role of snow interception in winter-time radiation processes of a coniferous sub-alpine forest, Hydrol. Process., 23, 2498–2512, 2009.
Strasser, U., Warscher, M., and Liston, G. E.: Modeling snow-canopy processes on an idealized mountain, J. Hydrometeorol., 12, 663–677, 2011.
Taconet, O., Bernard, R., and Vidal-Madjar, D.: Evapotranspiration over an agricultural region using a surface flux/temperature model based on NOAA-AVHRR data, J. Clim. Appl. Meteorol., 25, 284–307, 1986.
Tribbeck, M. J., Gurney, R. J., Morris, E. M., and Pearson, D. W.: A new Snow-SVAT to simulate the accumulation and ablation of seasonal snow cover beneath a forest canopy, J. Glaciol., 50, 171–182, 2004.

Tribbeck, M., Gurney, R., and Morris, E.: The radiative effect of a fir canopy on a snowpack, J. Hydrometeorol., 7, 880–895, 2006.
Tyler, N.: Climate, snow, ice, crashes, and declines in populations of reindeer and caribou (*Rangifer tarandus* L.), Ecol. Monogr., 80, 197–219, 2010.
Vikhamar-Schuler, D., Hanssen-Bauer, I., Schuler, T., Mathiesen, S., and Lehning, M.: Use of a multilayer snow model to assess grazing conditions for reindeer, Annals Glaciol., 54, 214–226, 2013.
Weiss, M., Baret, F., Smith, G., Jonckheere, I., and Coppin, P.: Review of methods for in situ leaf area index (LAI) determination: Part II. Estimation of LAI, errors and sampling, Agr. Forest Meteorol., 121, 37–53, 2004.
Wever, N., Fierz, C., Mitterer, C., Hirashima, H., and Lehning, M.: Solving Richards Equation for snow improves snowpack meltwater runoff estimations in detailed multi-layer snowpack model, The Cryosphere, 8, 257–274, doi:10.5194/tc-8-257-2014, 2014.
Yamazaki, T.: A one-dimensional land surface model adaptable to intensely cold regions and its applications in eastern Siberia, J. Meteorol. Soc. Jpn., 79, 1107–1118, 2001.
Yamazaki, T. and Kondo, J.: The snowmelt and heat balance in snow-covered forested areas, J. Appl. Meteorol., 31, 1322–1327, 1992.
Zappa, M., Pos, F., Strasser, U., Warmerdams, P., and Gurtz, J.: Seasonal water balance of an Alpine catchment as evaluated by different methods for spatially distributed snowmelt modelling, Nord. Hydrol., 34, 179–202, 2003.

GMDD
8, 209–262, 2015
A two-layer canopy with thermal inertia
I. Gouttevin et al.

Table 1. Parameters used by the SNOWPACK canopy module.

	Parameter (unit)	Description	value
Model internal parameters	i_{max} (mm m^{-2})	Coefficient for the maximum interception capacity	Spruce: 5.9 Pine: 6.6
	i_{LAI} (mm m^{-2})	Maximum interception of water by canopy per unit of LAI6Snow: $i_{max}(0.27+46/\rho_{s,\,int})$	Rain: 0.25
	k_{LAI} (–)	Extinction coefficient for SW and LW radiations	[0.4–0.8] default: 0.75
	f_{LAI} (–)	Fraction of LAI in the uppermost canopy layer for 2LHM only	default: 0.5
	D_{can} (m)	Average canopy diameter	1
	$\alpha_{wet,\,snow}$ (–)	Snow-covered canopy albedo	0.3
	$\alpha_{dry} = \alpha_{wet,\,rain}$ (–)	Dry and wet canopy albedo	0.11
	α_{trunk} (–)	Inner canopy layer albedo	0.09
	f_d (–)	Ratio d/z_{can}	2/3
	f_{z0m} (–)	Ratio z_{0m}/z_{can}	0.1
	$f_{z0h/z0m}$ (–)	Ratio z_{0h}/z_{0m}	0.999
	$r_{a,\,LAI}$ (–)	Parameter for the excess resistance introduces by canopy between surface and reference level	3.
	$f_{ra,\,snow}$	Factor for increased aerodynamic resistance for evaporation of intercepted snow	10
	$\rho_{biomass}$ (kg m^{-3})	Bulk biomass density	900
	$c_{p_{biomass}}$ (J kg^{-1} K^{-1})	Bulk biomass heat capacity	2800
	e_{leaf} (m)	Mean leaf (or needle) thickness. For 2LHM only	0.001
User-provided parameters	z_{can} (m)	Mean canopy height	
	LAI (m^2 m^{-2})	One-sided mean stand leaf-area index	
	c_f (–)	Direct throughfall fraction	
	B (m^2 m^{-2})	Stand basal area. For 2LHM only	

GMDD
8, 209–262, 2015

GMDD
8, 209–262, 2015

Table 2. Model versions and their calibration/optimization parameters.

Model version	Heat Mass represented	Number of canopy layers	Calibration parameters
1LnoHM	No	1	k_{LAI}
1LHM	Yes	1	k_{LAI}
2LHM	Yes	2	k_{LAI} f_{LAI}
1LHM*	Yes	1	k_{LAI} HM_{can}
2LHM*	Yes	2	k_{LAI} f_{LAI} HM_{trunk}

Table 3. Model performance upon calibration and optimization over 2003–2004. The calibration criterion CC is highlighted. The * denotes versions where heat mass is optimized and not physically derived.

Model version	Bestfit parameter	Calibration over 2003–2004									
		Results over 2003–2004					Results over 2003–2007				
		RMSE LW	MB LW	RMSE SW	MB SW	CC	RMSE LW	MB LW	RMSE SW	MB SW	CC
1LnoHM	$k_{LAI} = 0.75$	14.1	−3.5	9.4	0.3	**27.3**	17.5	−9.5	9.1	1.4	**37.5**
1LHM	$k_{LAI} = 0.75$	11.5	−2.5	9.4	0.3	**23.6**	14.5	−10.6	9.2	1.8	**36.0**
2LHM	$f_{LAI} = 0.5$ $k_{LAI} = 0.75$	8.3	−0.7	9.3	0.2	**18.4**	9.6	−6.7	9.1	1.6	**27.0**
1LHM*	$k_{LAI} = 0.8$ $HM_{can} = 90$	8.7	−0.7	9.4	−0.8	**19.3**					
2LHM*	$k_{LAI} = 0.75$ $f_{LAI} = 0.6$ $HM_{trunk} = 60$	7.9	0.1	9.3	0.2	**17.5**					

GMDD
8, 209–262, 2015

A two-layer canopy with thermal inertia

I. Gouttevin et al.

Table 4. Model performances upon calibration and optimization over 2003–2007.

Model version	Bestfit parameter	Calibration over 2003–2007									
		Results over 2003–2004					Results over 2003–2007				
		RMSE LW	MB LW	RMSE SW	MB SW	CC	RMSE LW	MB LW	RMSE SW	MB SW	CC
1LnoHM	$k_{LAI} = 0.75$	13.4	−2.4	9.4	−0.9	**26.2**	17.2	−9.1	9.0	0.2	**27.3**
1LHM	$k_{LAI} = 0.85$	11.4	−1.7	9.8	−1.8	**24.8**	14.2	−9.8	9.2	−0.5	**33.8**
2LHM	$k_{LAI} = 0.85$ $f_{LAI} = 0.5$	8.2	0.3	9.8	−1.8	**18.7**	9.1	−5.8	9.2	−0.6	**24.8**

GMDD
8, 209–262, 2015

A two-layer canopy with thermal inertia

I. Gouttevin et al.

GMDD
8, 209–262, 2015

A two-layer canopy with thermal inertia

I. Gouttevin et al.

Table 5. Statistics of model evaluation at Norunda. "corr" is the correlation coefficient.

Field data	Trunk temperature at 1.5 m (K)			Biomass heat flux ($W\,m^{-2}$)		Biomass + air heat storage flux ($W\,m^{-2}$)	
Model version	MB	RMSE	corr	RMSE	corr	RMSE	corr
1LnoHM	−0.41	1.7	0.88	16.3	0.	24.2	0.
1LHM	−0.05	1.6	0.92	24.5	0.79	18.9	0.86
2LHM	0.05	1.1	0.96	15.7	0.88	11.3	0.92

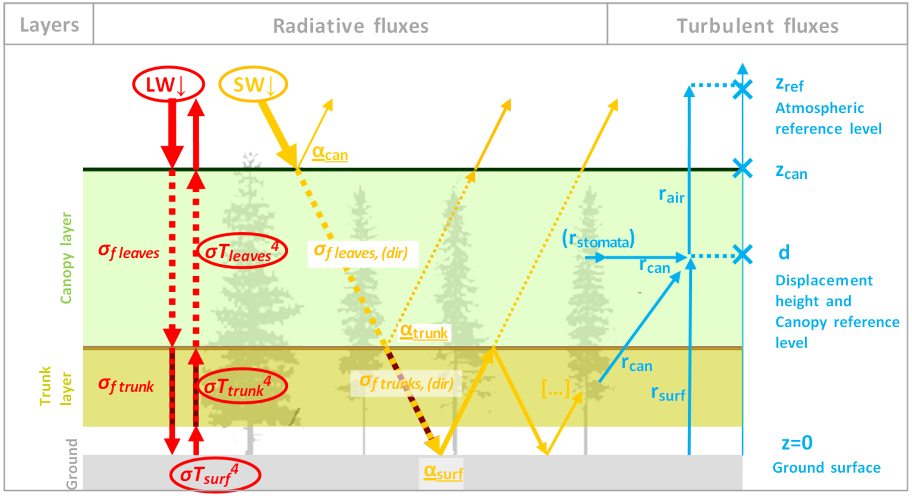

Figure 1. Radiative and turbulent fluxes in the 2-layer canopy module. Circles feature radiation sources, dashed lines indicate radiation absorption within the layer with the mentioned absorption factor; reflection factors at the border between layers are underlined. For turbulent fluxes, arrows denote aerodynamic resistance.

GMDD
8, 209–262, 2015

A two-layer canopy with thermal inertia

I. Gouttevin et al.

Title Page
Abstract | Introduction
Conclusions | References
Tables | Figures
◀| |▶
◀ ▶
Back | Close
Full Screen / Esc
Printer-friendly Version
Interactive Discussion

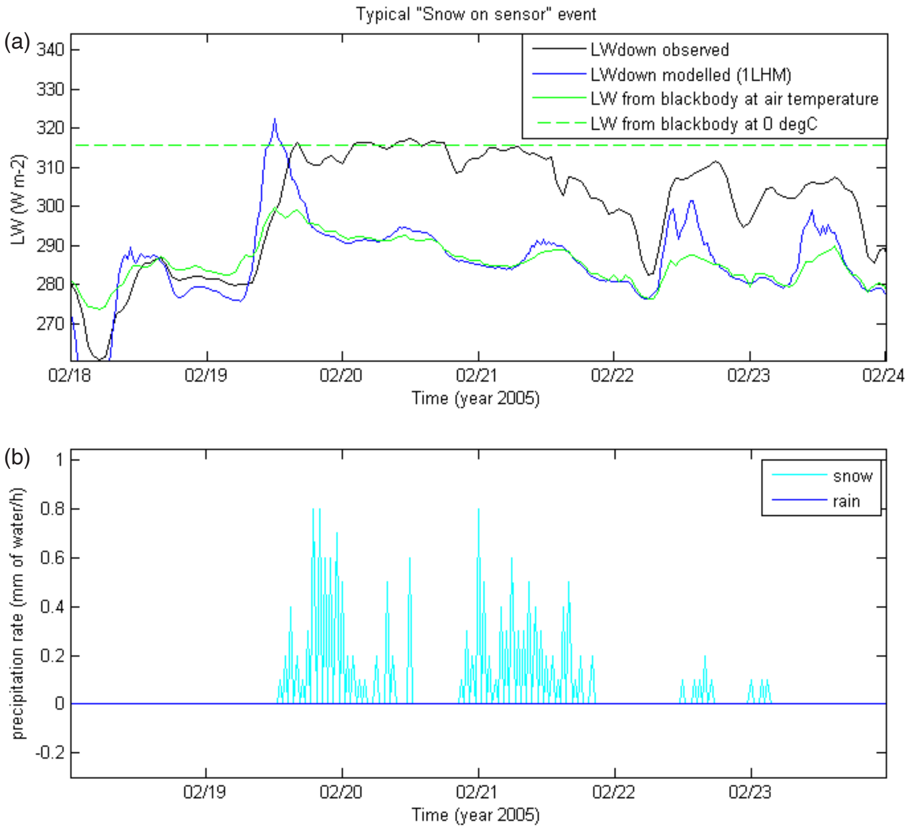

Figure 2. Typical event when snow-on-sensor is suspected. **(a)** Observed and modelled $LW{\downarrow}_{BC}$. **(b)** Observed precipitation record.

GMDD
8, 209–262, 2015

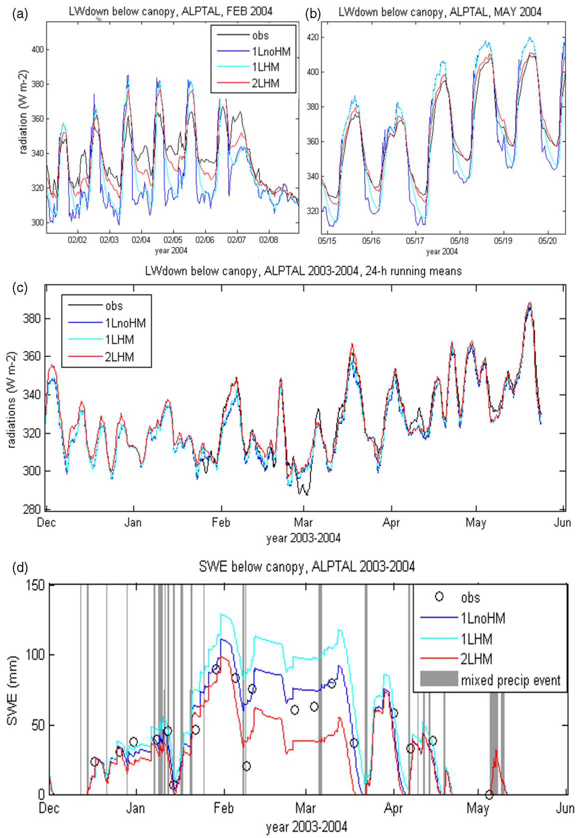

Figure 3. $LW{\downarrow}_{BC}$ and SWE as represented by the different model versions over the calibration period. **(a, b)** Subsets of daily cycles. **(c)** 24 h running means over the calibration period. **(d)** SWE.

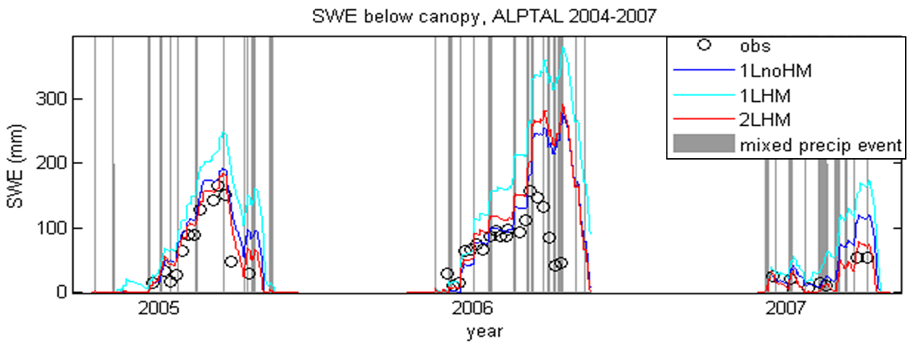

Figure 4. Sub-canopy SWE at Alptal over 2004–2007.

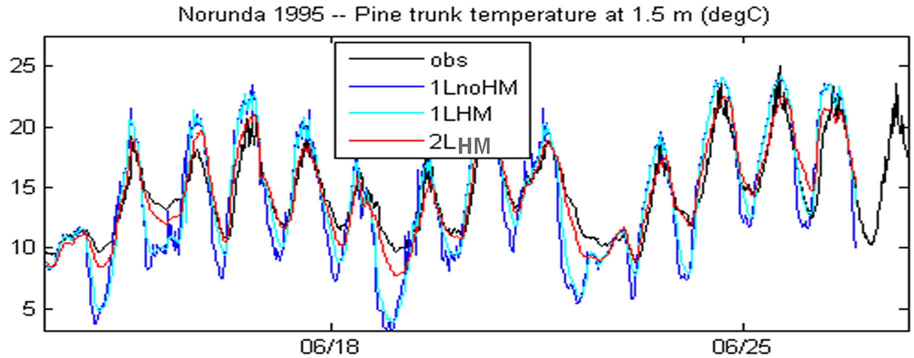

Figure 5. Comparison between observed Pine trunk temperature at 1.5 m height, 1 cm deep into the trunk, and modelled canopy temperatures: bulk canopy temperature for 1LnoHM and 1LHM, lowermost canopy-layer temperature for 2LHM.

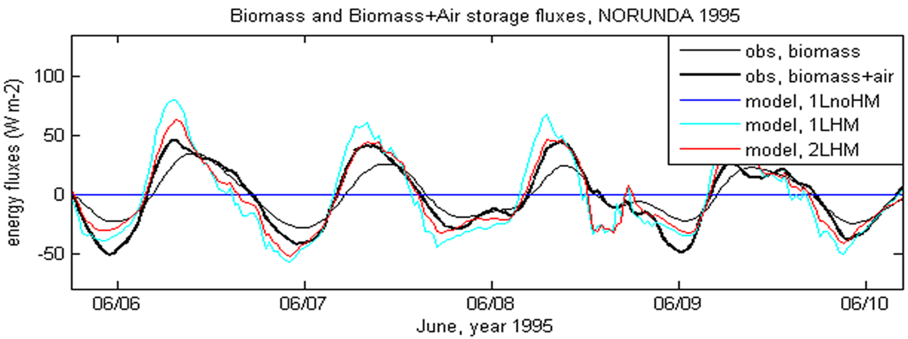

Figure 6. Comparison between biomass (and biomass + air) storage fluxes inferred from observations (obs) and biomass fluxes modelled by the different SNOWPACK versions (model) at Norunda.

GMDD
8, 209–262, 2015

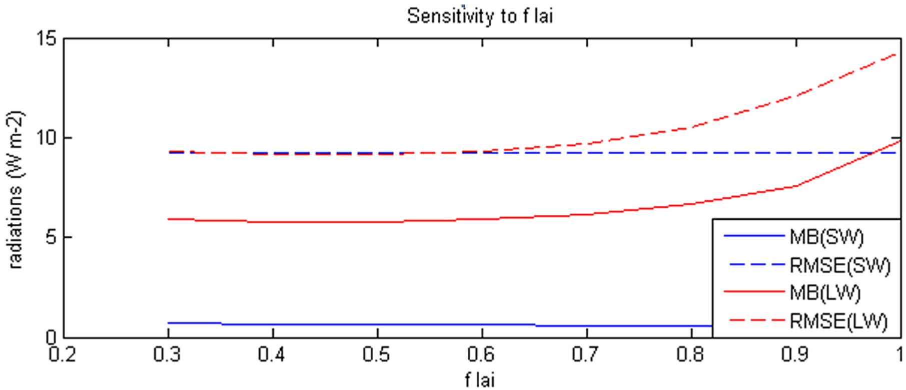

Figure 7. Sensitivity of model performance over 2003–2007 (with $k_{\mathrm{LAI}} = 0.85$) to f_{LAI}. The MB and RMSE are for the variables $\mathrm{SW}{\downarrow}_{\mathrm{BC}}$ (SW in the legend) and $\mathrm{LW}{\downarrow}_{\mathrm{BC}}$ (LW in the legend).

GMDD
8, 209–262, 2015

A two-layer canopy with thermal inertia

I. Gouttevin et al.